Upper-Bound Limit Analysis of the Multi-Layer Slope Stability and Failure Mode Based on Generalized Horizontal Slice Method

Huawei Zhang [1, 2], **Changdong Li** [*2, 3], **Wenqiang Chen**[2], **Ni Xie**[2], **Guihua Wang**[2],
Wenmin Yao[4], **Xihui Jiang**[2], **Jingjing Long**[2]

1. *Key Laboratory of Geotechnical Mechanics and Engineering of Ministry of Water Resources, Changjiang River Scientific Research Institute, Wuhan 430010, China*
2. *Faculty of Engineering, China University of Geosciences, Wuhan 430074, China*
3. *Badong National Observation and Research Station of Geohazards, China University of Geosciences, Wuhan 430074, China*
4. *School of Civil Engineering, Zhengzhou University, Zhengzhou 450001, China*

Huawei Zhang: https://orcid.org/0000-0003-1483-1924; Changdong Li: https://orcid.org/0000-0001-7902-7828

ABSTRACT: Multi-layer slopes are widely found in clay residue receiving fields. A generalized horizontal slice method (GHSM) for assessing the stability of multi-layer slopes that considers the energy dissipation between adjacent horizontal slices is presented. In view of the upper-bound limit analysis theory, the energy equation is derived and the ultimate failure mode is generated by comparing the sliding surface passing through the slope toe (mode A) with that below (mode B). In addition, the influence of the number of slices on the stability coefficients in the GHSM is studied and the stable value is obtained. Compared to the original method (Chen's method), the GHSM can acquire more precise results, which takes into account the energy dissipation in the inner sliding soil mass. Moreover, the GHSM, limit equilibrium method (LEM) and numerical simulation method (NSM) are applied to analyze the stability of a multi-layer slope with different slope angles and the results of the safety factor and failure mode are very close in each case. The ultimate failure modes are shown to be mode B when the slope angle is not more than 28°. It illustrates that the determination of the ultimate sliding surface requires comparison of multiple failure modes, not only mode A.

KEY WORDS: stability and failure mode, slope stability, generalized horizontal slice method, upper-bound limit analysis, energy dissipation, geotechnical engineering.

0 INTRODUCTION

The Shenzhen Hong'ao Landslide of December 20, 2015 in Southeast China killed 77 people and buried or damaged 33 buildings (Gao et al., 2017). Rapid urbanization generates a large amount of clay residue that is deposited in receiving fields, forming multi-layer slopes. The clay residue slopes are close to cities and have serious consequences if unstable, thus the stability of which is being increasingly emphasized.

Slope stability analysis is a classic subject in geotechnical engineering (Fang et al., 2023; Su et al., 2022; Tang et al., 2022; Cui et al., 2021;Li et al., 2021, 2019; Wang et al., 2020). At present, limit equilibrium methods (LEM) such as the Swedish circle method (Fellenius, 1927) and Bishop method (Bishop, 1955) are the most widely used methods in engineering due to their simplicity and convenience. However, the kinematic

problem of soil mass failure remains to be solved because the slope soil mass is regarded as a statically indeterminate structure in these methods (Zhou et al., 2024; Kamran et al., 2023; Chen et al., 2021; Li et al., 2020; Lim et al., 2017). Targeting the problems, Drucker et al. (1952) proposed the theory of limit analysis, and Wai-Fah Chen and his colleagues (Chen and Liu, 1990; Chen and Sawada, 1983; Chen, 1975; Chen and Giger, 1971) introduced this theory into slope stability with a strictly theoretical basis and physical significance; this method has been widely promoted by many researchers (Chen et al., 2020; Li et al., 2010; Ausilio et al., 2001; Michalowski and You, 2000; Michalowski, 1998; Chang et al., 1984). Chen's method (Chen, 1975) assumes that the sliding surface is a log-spiral and the sliding soil mass is one rigid body without considering its internal energy dissipation. However, the sliding soil mass corresponding to the different polar angles needs to experience deformation to accommodate the changing curvature of the log-spiral, which is not consistent with the above assumption of a single rigid body (Wang et al., 2020; Yan et al., 2019; Liu et al., 2017).

To solve the aforementioned problem, a vertical slice method was proposed by Michalowski (1995), which divides

the sliding soil mass into several vertical slices so that the soil can adapt to the corresponding curvature of the log-spiral. Based on the rotational failure mechanism, this method transforms the sliding movement into translational movement and considers the energy dissipation between the vertical slices. In addition, Chen et al. (2017) presented a polar slice method that divides the sliding soil mass into several small blocks with one polar point in the rotational failure mechanism and the energy dissipation between the adjacent blocks is considered to assess the slope stability. The results were compared with those of Chen's method and the vertical slice method.

Multi-layer slopes, such as clay residue receiving fields slopes, have been widely found in the world (Zhang et al., 2023; Zhong et al., 2023; Farshidfar et al., 2020; Guo and Griffiths, 2020; Li and Jiang, 2020; Wang and Huang, 2020; Qin and Chian, 2017). This type of artificial slope is formed by layered filling and then compaction, in which the soil properties, for instance, weight and the soil shear strength index, exhibit obvious layered characteristics. If the vertical and polar slice methods are used to divide a sliding soil mass, the inner sliding soil mass is greatly affected by changes in the soil properties, which complicates the calculations. To improve this, the horizontal slice method was presented to assess the slope stability (Lo and Xu, 1992), and further studies have been conducted by other researchers (Zhou et al., 2020; Kumar and Samui, 2006; Shahgholi et al., 2001). However, in the upper-bound limit analysis, for multi-layer slopes where the sliding surfaces are mostly assumed to pass through the slope toe without considering the condition of passing below the slope toe. Therefore, a generalized horizontal slice method (GHSM) is proposed to evaluate the slope stability considering the energy dissipation between the adjacent horizontal slices in this paper; this method determines the ultimate failure mode by comparing the stability coefficients of sliding surface passing through the slope toe with that below it. Compared to the original method (Chen's method), the GHSM can acquire more precise results, which takes into account the energy dissipation in the inner sliding soil mass. Moreover, the GHSM, LEM and numerical simulation method (NSM) are applied to analyze the stability of a multi-layer slope and explore the effect of slope angle on the stability and failure mode.

1   PRINCIPLES OF THE GHSM

1.1   Upper-Bound Limit Analysis

In this study, the upper-bound limit analysis is adopted to assess the slope stability which shows that the external rate of work is less than or equal to the rate of internal energy dissipation (Shield and Drucker, 1953). The internal energy dissipation includes the energy dissipation of the inner sliding soil mass and the sliding surface. To calculate the energy dissipation of the inner sliding soil mass, it is necessary to assume that the soil mass obeys the law of associated flow to obtain the velocity fields between the adjacent horizontal slices. In the GHSM, the sliding surface is composed of a series of log-spirals with one pole, so its energy dissipation can be obtained by summing the integrals of partitioned log-spirals. In addition, the external work consists of the work of the soil weight and seismic force. The rates of the work of the soil weight and seis-

mic force can both be calculated by summing the integrals of the divided sliding soil mass. Therefore, based on the upper-bound limit analysis, the slope stability coefficient can be obtained by the equation between the external rate of work and the internal rate of energy dissipation.

1.2   Multi-Layer Slope Model Based on GHSM

When clay residue is transported to a clay residue receiving field to be filled, it usually needs to be horizontally compacted by rollers, thus resulting in a multi-layer slope. As shown in Figure 1a, a typical clay residue receiving field slope in Shenzhen, has distinct structural layering characteristics, and the physical and mechanical properties of each soil layer are distinctly different. Based on the practical slope model in Figure 1a, a simplified multi-layer slope model is generated as shown in Figure 1b. The GHSM divides the sliding soil mass into several horizontal slices and the potential sliding surface is composed of a series of log-spirals with one pole (O). The points on the potential sliding surface are represented by polar radius (r) and angle (θ) with respect to polar point O. Additionally, not only the energy dissipation of the sliding surface is calculated, but also the energy dissipation of the inner sliding soil mass is considered.

1.3   Coordinate Calculations

As shown in Figure 2, the rectangular coordinate system is established with point A, which emerges from the ground as the origin. The slope height is H and the surface is represented as a series of $\overline{C_{i-1}C_i}$ ($i = 1,2,...,n$). The sliding soil mass above the ground is divided into N horizontal layers and layer i with height h_i and strength parameters (c_i, φ_i, γ_i) ($i = 1,2,\cdots,n$), which under the ground is treated as one whole layer with strength parameters (c_0, φ_0, γ_0). The potential sliding surface is composed of a series of log-spirals $\widehat{B_{i-1}B_i}$ ($i = 1,2,...,n$) and log-spiral $\widehat{AB_0}$ with polar point $O(x_O, y_O)$. To facilitate the solution, the horizontal blocks are divided and region $B_nB_{n-1}C_{n-1}C_n$ is taken as an example. Region $B_nB_{n-1}C_{n-1}C_n$ is divided into triangle $B_nB_{n-1}C_{n-1}$, triangle $B_nC_{n-1}C_n$, and region B_nB_{n-1}, which are obtained by region OB_nB_{n-1} minus triangle OB_nB_{n-1}. Region AB_0 is calculated by region OAB_0 minus triangle OAB_0. The points E, F_n, G_n, and H_n are the centers of gravity of the triangles OAB_0, $B_nB_{n-1}C_{n-1}$, $B_nC_{n-1}C_n$, and OB_nB_{n-1}, and their coordinates can be acquired by the coordinates of A, B_n, C_n, and O.

Suppose that the polar angles θ_0 and θ_1 of the points B_0 and B_1, the distance L between point A and point C_0, which is the toe of the slope, are known.

Using the variable optimization method of Chen et al. (2017), all the other coordinates of the blocks are obtained.

The relationship between the vertical coordinates y_B^0 and y_B^1 of points B_0 and B_1 in the first horizontal block is expressed by Eq. (1)

$$y_B^1 - y_B^0 = r_0 \sin \theta_0 - r_1 \sin \theta_1 = h_1 \tag{1}$$

Based on the log-spiral equation, the polar radii r_0 and r_1 of the points B_0 and B_1 satisfy Eq. (2)

$$r_0 = r_1 \exp\left[\tan\varphi_1(\theta_0 - \theta_1)\right] \tag{2}$$
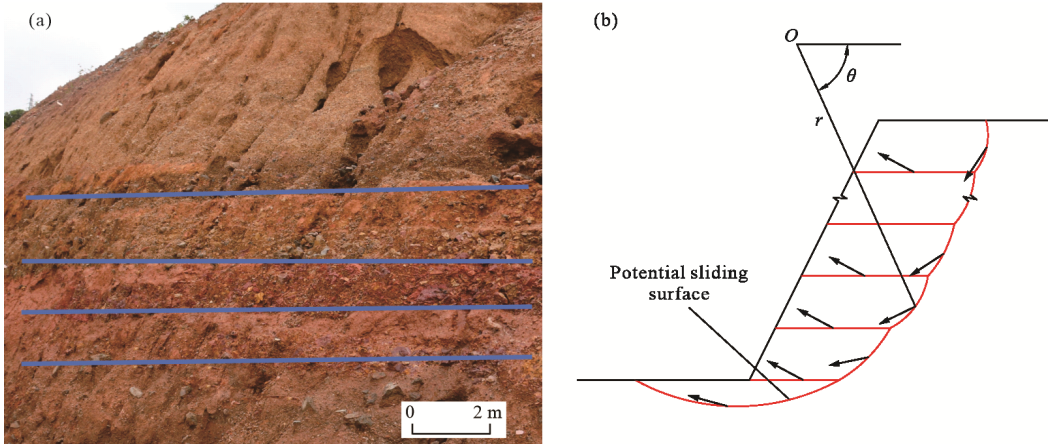
Figure 1. Practical and simplified slope models; (a) a typical clay residue receiving field slope in Shenzhen, China; (b) a simplified multi-layer slope model.
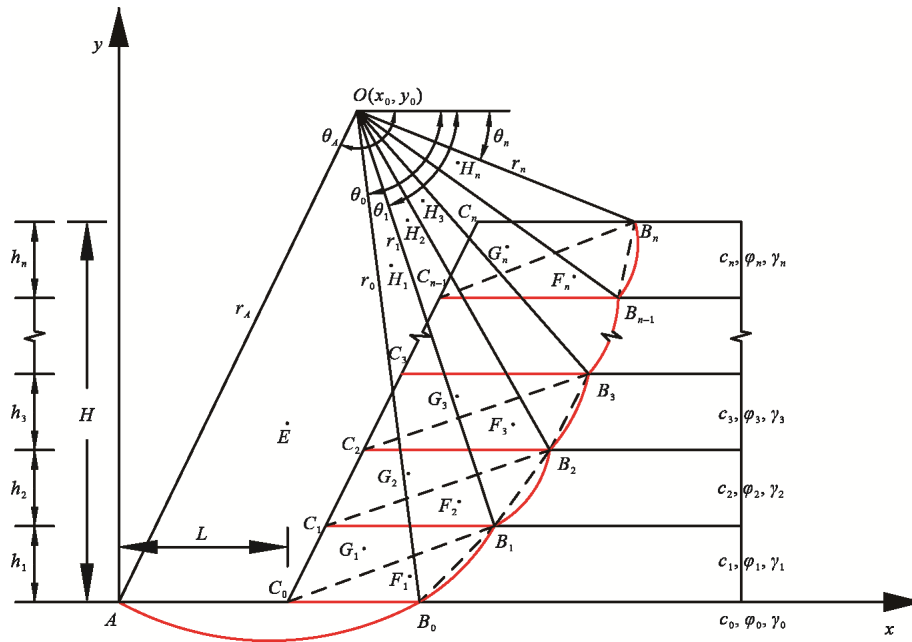

Figure 2. The schematic diagram of the principle of the GHSM.

Through the combination of Eqs. (1) and (2), the polar radii r_0 and r_1 are calculated.

Similarly, the polar angles θ_{i-1}, θ_i and polar radii r_{i-1}, r_i of the points B_{i-1}, B_i in the horizontal block i satisfy Eq. (3)

$$\left. \begin{aligned} r_{i-1} &= r_i \exp\left[\tan\varphi_i\left(\theta_{i-1} - \theta_i\right)\right] \\ r_{i-1}\sin\theta_{i-1} - h_i &= r_i\sin\theta_i \\ (i &= 2,3,...,n) \end{aligned} \right\} \tag{3}$$

Through the division of both sides of Eq. (3) and the elimination of the variable r_i, Eq. (4) can be obtained

$$\frac{r_{i-1}}{r_{i-1}\sin\theta_{i-1} - h_i} = \frac{\exp\left[\tan\varphi_i\left(\theta_{i-1} - \theta_i\right)\right]}{\sin\theta_i}(i = 2,3,...,n) \tag{4}$$

According to Eq. (4), the polar angle θ_i can be obtained when the polar angle θ_{i-1} and the polar radius r_{i-1} are known.

The polar radius r_i is determined by Eq. (5)

$$r_i = r_{i-1}\exp\left[\tan\varphi_i\left(\theta_i - \theta_{i-1}\right)\right](i = 2,3,...,n) \tag{5}$$

Through the combination of Eqs. (4) and (5) and the performance of an iterative calculation, the θ_i and r_i of point B_i ($i = 2,3,\cdots,n$) are calculated.

The vertical coordinates y_A and y_B^0 of points A and B_0 are equal, and the polar radii r_A and r_0 of points A and B_0 satisfy the log-spiral equation. The relationship between points A and B_0 is expressed as follows

$$\left. \begin{aligned} r_A\sin\theta_A &= r_0\sin\theta_0 \\ r_A &= r_0\exp\left[\tan\varphi_0\left(\theta_A - \theta_0\right)\right] \end{aligned} \right\} \tag{6}$$

The polar radius r_A and polar angle θ_A of point A are calculated by Eq. (6).

The coordinates of polar point O can be determined by Eq. (7)

$$\left. \begin{aligned} x_0 &= x_A - r_A\cos\theta_A \\ y_0 &= y_A + r_A\sin\theta_A \end{aligned} \right\} \tag{7}$$

where $x_A = 0$ and $y_A = 0$.

The coordinates of B_i are obtained by Eq. (8)

$$\left.\begin{array}{r} x_B^i = x_0 + r_i\cos\theta_i\,(i = 0,...,n) \\ y_B^0 = 0\,(i = 0) \\ y_B^i = \sum_1^i h_i\,(i = 1,...,n) \end{array}\right\} \quad (8)$$

The horizontal and vertical coordinates of C_i with different slope angle β are calculated using Eq. (9)

$$\left.\begin{array}{r} x_C^0 = L\,(i = 0) \\ y_C^0 = 0\,(i = 0) \\ x_C^i = L + \dfrac{\sum_1^i h_i}{\tan\beta}\,(\beta \neq 90°)\,(i = 1,...,n) \\ x_C^i = L\,(\beta = 90°)\,(i = 1,...,n) \\ y_C^i = \sum_1^i h_i\,(i = 1,...,n) \end{array}\right\} \quad (9)$$

1.4 Energy Equation

The external rate of work and the internal rate of energy dissipation would be calculated, the expressions of various powers are shown in Table 1.

The values of the cohesion c_{int}^i and the internal friction angle φ_{int}^i of the interface are assumed to be the smaller values out of the values of the two corresponding blocks.

The velocity V_n of block $B_n B_{n-1} C_{n-1} C_n$ is determined by the velocity of the intersection point between the angle bisector of $\angle B_{n-1}OB_n$ and the log-spiral. Therefore, the value of the velocity can be obtained as Eq. (10)

$$V_n = r_n \exp\left[\tan\varphi_n\left(\frac{\theta_n + \theta_{n-1}}{2} - \theta_n\right)\right]\omega \quad (10)$$

where ω is the angle velocity to the polar point O.

In terms of the interfaces above the ground, the relationship of the velocity vectors is shown in Figure 3.

The values of the angle of the velocity vector triangle above the ground are expressed by Eq. (11)

$$\left.\begin{array}{l} X = \dfrac{\pi}{2} + \dfrac{\theta_n + \theta_{n-1}}{2} - \varphi_{int}^{n-1} \\ Y = \dfrac{\pi}{2} - \dfrac{\theta_{n-1} + \theta_{n-2}}{2} + \varphi_{int}^{n-1} \\ Z = \dfrac{\theta_{n-2} - \theta_n}{2} \end{array}\right\} \quad (11)$$

Table 1 The expressions of various powers (modified from Xia and Chen, 2018)

Powers	Above the ground	Under the ground
P_W	$P_W^i = P_{\Delta B_{i-1}B_iC_{i-1}}^W + P_{\Delta B_iC_{i-1}C_i}^W + P_{\mathrm{Region}OB_{i-1}B_i}^W - P_{\Delta OB_{i-1}B_i}^W$ $P_{\Delta B_{i-1}B_iC_{i-1}}^W = 0.5\gamma_i h_i\left(x_B^{i-1} - x_C^{i-1}\right)\left(x_F^i - x_0\right)\omega$ $P_{\Delta B_iC_{i-1}C_i}^W = 0.5\gamma_i h_i\left(x_B^i - x_C^i\right)\left(x_G^i - x_0\right)\omega$ $P_{\Delta OB_{i-1}B_i}^W = 0.5\gamma_i r_{i-1} r_i \sin\left(\theta_{i-1} - \theta_i\right)\left(x_{H_i} - x_0\right)\omega$ $P_{\mathrm{Region}OB_{i-1}B_i}^W = \gamma_i r_i^3 f_1 \omega$ $(i = 1,2,\cdots,n)$	$P_W^0 = P_{\mathrm{Region}OAB_0}^W - P_{\Delta OAB_0}^W$ $P_{\Delta OAB_0}^W = 0.5\gamma_0 r_A r_B \sin\left(\theta_A - \theta_0\right)\left(x_E - x_0\right)\omega$ $P_{\mathrm{Region}OAB_0}^W = \gamma_0 r_A^3 f_2 \omega$
P_k	$P_k^i = P_{\Delta B_{i-1}B_iC_{i-1}}^k + P_{\Delta B_iC_{i-1}C_i}^k + P_{\mathrm{Region}OB_{i-1}B_i}^k - P_{\Delta OB_{i-1}B_i}^k$ $P_{\Delta B_{i-1}B_iC_{i-1}}^k = 0.5\gamma_i h_i\left(x_B^{i-1} - x_C^{i-1}\right)\left(y_0 - y_F^i\right)\omega k_h$ $P_{\Delta B_iC_{i-1}C_i}^k = 0.5\gamma_i h_i\left(x_B^i - x_C^i\right)\left(y_0 - y_G^i\right)\omega k_h$ $P_{\Delta OB_{i-1}B_i}^k = 0.5\gamma_i r_{i-1} r_i \sin\left(\theta_{i-1} - \theta_i\right)\left(y_0 - y_H^i\right)\omega k_h$ $P_{\mathrm{Region}OB_{i-1}B_i}^k = \gamma_i r_i^3 f_3 \omega k_h$ $(i = 1,2,\cdots,n)$	$P_k^0 = P_{\mathrm{Region}OAB_0}^k - P_{\Delta OAB_0}^k$ $P_{\Delta OAB_0}^k = 0.5\gamma_0 r_A r_B \sin\left(\theta_A - \theta_0\right)\left(y_0 - y_E\right)\omega k_h$ $P_{\mathrm{Region}OAB_0}^k = \gamma_0 r_A^3 f_4 \omega k_h$
P_S	$P_S^i = c_i r_i^2 \omega \dfrac{\exp\left[2\tan\varphi_i\left(\theta_{i-1} - \theta_i\right)\right] - 1}{2\tan\varphi_i}$ $(i = 1,2,\cdots,n)$	$P_S^0 = c_0 r_A^2 \omega \dfrac{\exp\left[2\tan\varphi_0\left(\theta_A - \theta_0\right)\right] - 1}{2\tan\varphi_0}$
P_I	$P_I^i = \left(x_B^i - x_C^i\right)c_{int}^i V_{int}^i \cos\varphi_{int}^i$ $(i = 1,2,\cdots,n-1)$	$P_I^0 = \left(x_B^0 - x_C^0\right)c_{int}^0 V_{int}^0 \cos\varphi_{int}^0$

P_W: the power of soil weight; P_k: the power of seismic force; P_S: the dissipation power of the sliding surface; P_I: the dissipation power of interfaces; k_h: the yield acceleration factor where only the horizontal component of the seismic coefficient is considered.

$$f_1 = \frac{\left(3\tan\varphi_i\cos\theta_{i-1} + \sin\theta_{i-1}\right)\exp\left[3\left(\theta_{i-1} - \theta_i\right)\tan\varphi_i\right] - 3\tan\varphi_i\cos\theta_i - \sin\theta_i}{3\left(1 + 9\tan^2\varphi_i\right)};$$

$$f_2 = \frac{\left(3\tan\varphi_0\cos\theta_A + \sin\theta_A\right)\exp\left[3\left(\theta_A - \theta_0\right)\tan\varphi_0\right] - 3\tan\varphi_0\cos\theta_0 - \sin\theta_0}{3\left(1 + 9\tan^2\varphi_0\right)};$$

$$f_3 = \frac{\left(3\tan\varphi_i\sin\theta_{i-1} - \cos\theta_{i-1}\right)\exp\left[3\left(\theta_{i-1} - \theta_i\right)\tan\varphi_i\right] - 3\tan\varphi_i\sin\theta_i + \cos\theta_i}{3\left(1 + 9\tan^2\varphi_i\right)};$$

$$f_4 = \frac{\left(3\tan\varphi_0\sin\theta_A - \cos\theta_A\right)\exp\left[3\left(\theta_A - \theta_0\right)\tan\varphi_0\right] - 3\tan\varphi_0\sin\theta_0 + \cos\theta_i}{3\left(1 + 9\tan^2\varphi_0\right)}.$$

Based on the sine rules of triangles, the value of the relative velocity V_{int}^{n-1} of the interface can be calculated by Eq. (12)

$$\frac{V_{\text{int}}^{n-1}}{\sin Z} = \frac{V_n}{\sin Y} \qquad (12)$$

The relationship of the velocity vectors for the interface at the ground is shown in Figure 4.

Point D is the intersection point between the angle bisector of $\angle AOB_0$ and the log-spiral.

The values of the angle of the velocity vector triangle at the ground are expressed by Eq. (13)

$$\left.\begin{array}{c} X = \dfrac{\pi}{2} + \dfrac{\theta_1 + \theta_0}{2} - \varphi_{\text{int}}^0 \\[2mm] Y = \dfrac{\pi}{2} - \dfrac{\theta_0 + \theta_A}{2} + \varphi_{\text{int}}^0 \\[2mm] Z = \dfrac{\theta_A - \theta_0}{2} \end{array}\right\} \qquad (13)$$

The value of the relative velocity V_{int}^0 of the interface $B_0 C_0$ can be calculated by Eq. (14)

$$\frac{V_{\text{int}}^0}{\sin Z} = \frac{V_1}{\sin Y} \qquad (14)$$

With the principle of energy conservation, in which the energy of the external force is equal to the energy dissipation, the energy equation of the upper-bound limit analysis can be obtained

$$P_W + P_k = P_S + P_I \qquad (15)$$

From the above equations, the energy equation of the upper-bound limit analysis of the sliding surface passing below the toe of the slope (mode B) can be established. When $L = 0$ in mode B, the energy equation of the upper-bound limit analysis of the sliding surface passing through the toe of the slope (mode A) is obtained.

On the basis of Eq. (15), the stability coefficients (including static safety factor F_s or yield acceleration factor k_h) can be minimized with respect to the three independent variables θ_0, θ_1 and L. In this paper, instability of slopes would either from reducing strength parameters or from seismic forces, but not
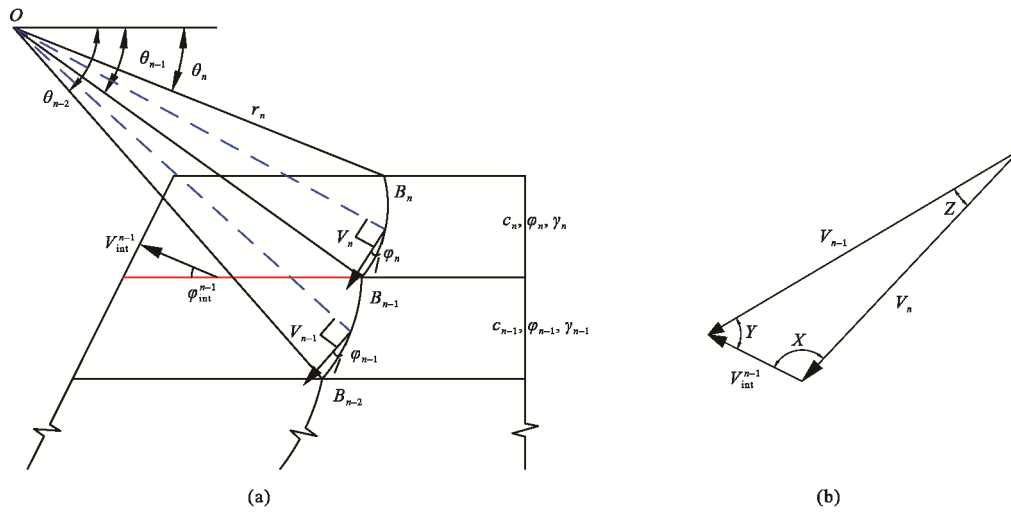

Figure 3. The relationship of velocity vectors above the ground; (a) schematic diagram of relative velocity and block velocity; (b) the triangle relationship with the three velocity vectors.
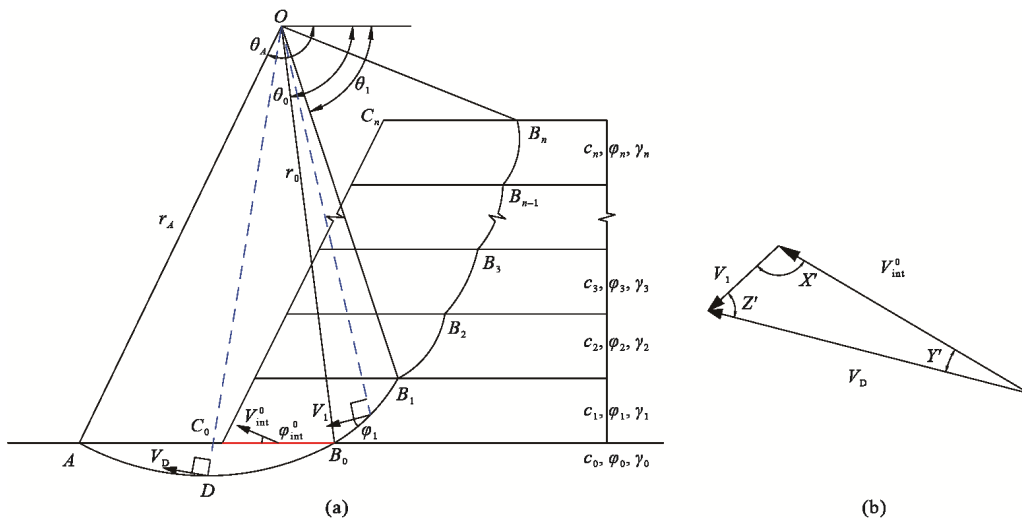

Figure 4. The relationship of velocity vectors at the ground; (a) schematic diagram of relative velocity and block velocity; (b) the triangle relationship with the three velocity vectors.

both, i.e., F_s and k_h are solved separately. The static safety factor F_s is defined using the shear strength reduction (SSR) technique, as shown in Eq. (16). The reduced shear strength parameters c_i' and φ_i' can be calculated below in Eq. (16).

$$F_s = \frac{c_i}{c_i{'}} = \frac{\tan\left(\varphi_i\right)}{\tan\left(\varphi_i{'}\right)} \qquad (16)$$

However, the mapping relationship between the stability coefficients and the independent variables is implicit, and the expressions are complex and cannot be solved directly by the analytical method. Therefore, a harmony search algorithm (Geem and Kim, 2001), which is a newly introduced heuristic global optimization algorithm, can be used to determine the stability coefficients (including F_s and k_h) and has been successfully used to address the optimization problem (Ma et al., 2022; Wang et al., 2013; Cheng et al., 2011).

The solution of the stability coefficients is implemented as a nonlinear constraint optimization problem, which are presented as follows

Minimize: F_s or k_h

$$\text{Subject to:} \begin{cases} P_W + P_k = P_S + P_I \\ 0 < \theta_i < \pi\,(i = 0,...,n) \\ \theta_i > \theta_{i-1}\,(i = 1,...,n) \\ 0 \leqslant L \leqslant 3H/\tan\beta \\ x_B^i \geqslant x_C^i\,(i = 0,...,n) \end{cases} \qquad (17)$$

The problem is solved by independent programming of MATLAB, and the flow chart is shown in Figure 5.

By trial and error, the stability coefficients can be obtained when the value of L is between zero and three times the

slope width, namely, $0 \leqslant L \leqslant 3H/\tan\beta$. When $\beta = 90°$, the range of the slope width L is $0 \leqslant L \leqslant 3H/\tan(75°)$.

2   CASE STUDIES

2.1   Case 1: Homogeneous Slope

In this section, the parameters of the slope are specified as follows: the slope height $H = 7$ m, slope angle $\beta = 60°$, unit weight $\gamma = 18$ kN/m³, cohesion $c = 12$ kPa, and internal frictional angle $\varphi = 25°$. The results (F_s or k_h) of the GHSM, polar slice method, vertical slice method, and Chen's method are marked with subscripts of 1, 2, 3, and 4, respectively, in this section.

The number of slices N in the GHSM directly affects the stability coefficient. The greater N is, the closer the stability coefficient is to the real value, but the larger the computational burden. Therefore, on the basis of ensuring the accuracy of the stability coefficients, a suitable value of N should be selected to reduce the number of calculations. Figure 6 shows the curves of the static safety factor F_{s1} and yield acceleration factor k_{h1} varying with N ranging from 2 to 12 in the two modes.

Both Figures 6a and 6b show that as N increases, the stability coefficients (including F_{s1} and k_{h1}) first present an upward trend and finally reach the steady state. Figure 6 shows that when N is not less than 8, the stability coefficients under modes A and B can reach stable values. In addition, the results of the static safety factor F_{s1} or the yield acceleration factor k_{h1} in Figure 6a are both smaller than those in Figure 6b, so mode A passing through the toe of the slope is the ultimate failure mode in this case.

Although the generalized horizontal, polar and vertical slice methods all use the slice method to divide the sliding soil mass that considers the energy dissipation between adjacent
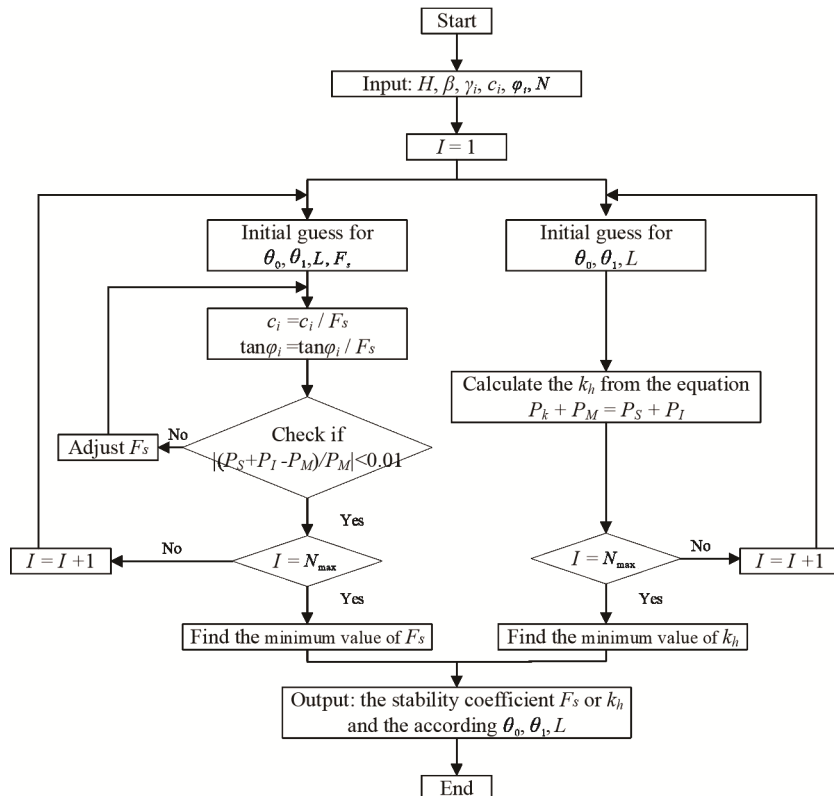

Figure 5. Flow chart for solving the results of stability coefficient.

slices, the type of slice method used is different, so it is necessary to compare and analyze the stability coefficient obtained by the three different methods. The stability coefficients (including F_s and k_h) of the three methods varying with N from 2 to 12 are shown in Figure 7. It shows that as N increases, first, the stability coefficients (including F_{s1} and k_{h1}, F_{s3} and k_{h3}) of the generalized horizontal and vertical slice methods trend upwards, while the stability coefficients (including F_{s2} and k_{h2}) of the polar slice methods trend downwards, which is explained by Chen et al. (2017). As N increases to a certain number, all the three slice methods all reach the steady state, and the stability coefficients finally reach stable values. The stable values of the GHSM are similar to those of the polar and vertical methods. Both Figures 7a and 7b show that when $N = 8$, the stability coefficients of the GHSM are stable, while this occurs at $N = 10$ for the polar and vertical slice methods.

According to the aforementioned parameters of the slope, the stability coefficients of the GHSM ($N = 8$), polar slice method ($N = 10$) and Chen's method are listed in Table 2. The stability coefficients of the GHSM are close to those of the polar slice method but greater than those of Chen's method, neglecting the energy dissipation in the inner sliding soil mass. Comparing the stability coefficients in the two modes, the ulti-

mate sliding surfaces are determined by mode A.

Moreover, Figure 8 shows the ultimate sliding surfaces of the three methods. Figure 8a shows the ultimate sliding surfaces by SSR, and the trailing edge of the ultimate sliding surface of the GHSM is near that of the polar slice method. Figure 8b shows the ultimate sliding surfaces induced by yield accelerations and presents the same phenomenon as Figure 8a.

2.2   Case 2: Multi-Layer Slope

Clay residue slopes are usually formed by layered filling and then compaction, so they have strongly layering properties. In addition, the GHSM is more suitable for analyzing the stability of multi-layer slopes because it is not affected by the variability in the soil properties, and the soil parameters of each block can be obtained directly, which facilitates the calculations.

A multi-layer slope located at a receiving field in Shenzhen, China, is used as an example to analyze slope stability and failure mode (derived from Wang, 2018). As shown in Figure 9, the slope height $H = 10$ m and contains 5 soil layers above the ground, in which the deposits thickness of each layer is 2 m. Layers 1–5 consist of clay residue generated from urban construction and layer 6 indicates the original ground consisting of silty clay. The values of the density ρ, cohesion c and internal
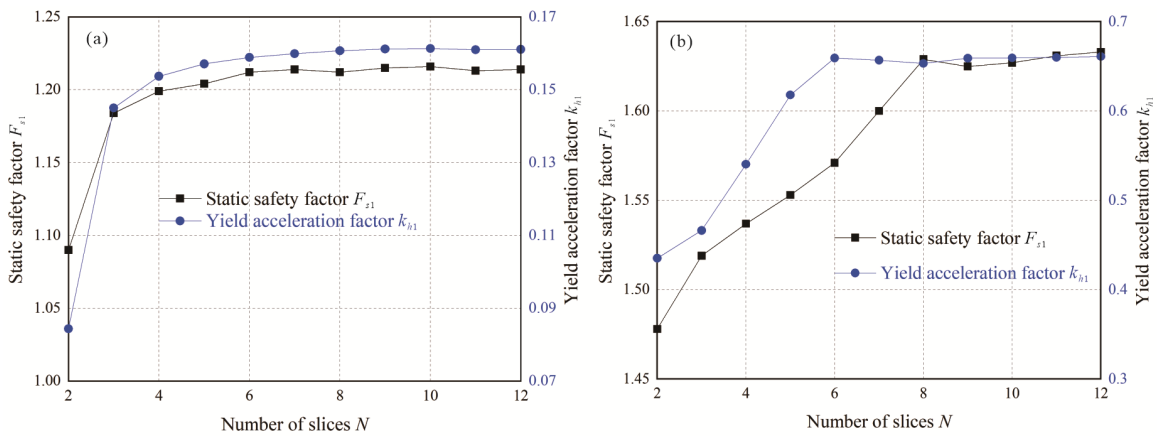

Figure 6. Influence of the number of slices N on F_{s1} and k_{h1} in two modes of rotational failure mechanisms; (a) mode A, passing through the toe of the slope; (b) mode B, passing below the toe of the slope.
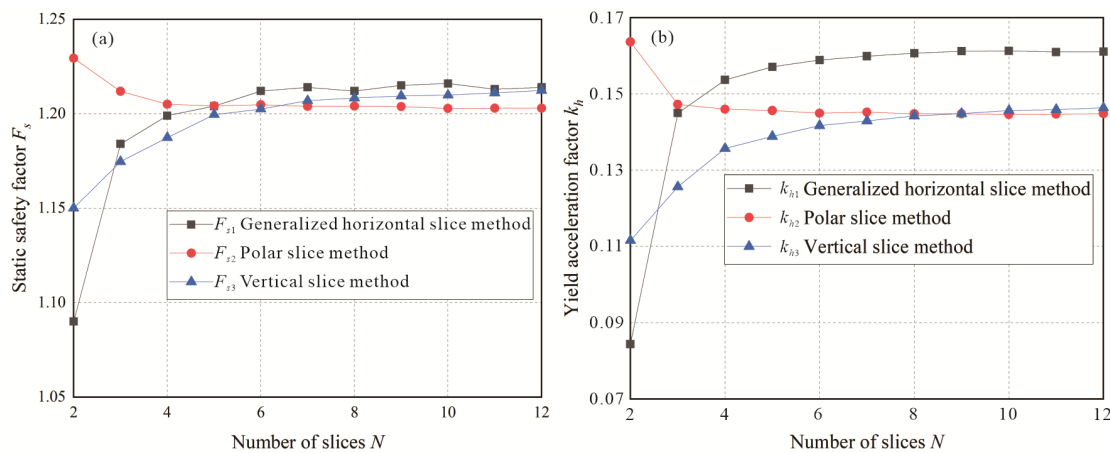

Figure 7. Comparison between generalized horizontal, polar and vertical slice methods (Chen et al., 2017); (a) static safety factor F_s; (b) yield acceleration factor k_h.
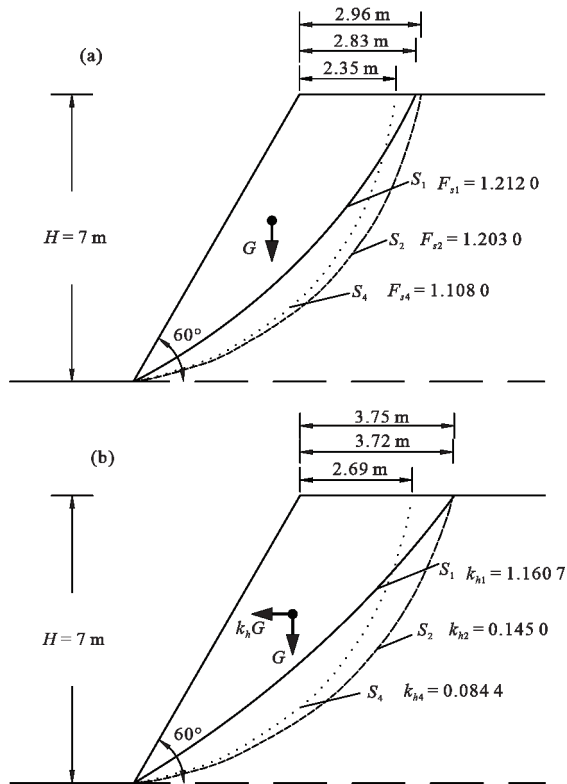
Figure 8. Ultimate sliding surfaces by GHSM, polar slice method and Chen's method (Chen et al., 2017); (a) static condition; (b) seismic condition.
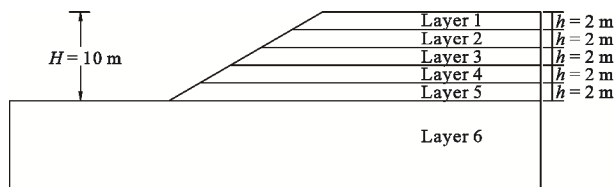

Figure 9. Model of the multi-layer slope (derived from Wang, 2018).

friction angle φ of the different layers can be seen in Table 3.

Based upon the above results, the number of slices $N \geqslant 8$ can ensure that value of the stability coefficient is stable, so $N = 10$ above the ground is selected for the GHSM calculations below; namely, the height of each block is 1 m.

Some researchers (Zhou et al., 2020; Kumar and Samui, 2006) adopt upper-bound limit analysis to study the stability of multi-layer slopes but focus only on the failure mode of passing through the slope toe (mode A). In this section, the GHSM is used with the soil parameters in Table 3. In each case, both failure modes A and B are calculated to determine the ultimate failure mode. The results of the safety factor are shown by the black line in Figure 10, and the ultimate sliding surface is presented by the yellow line in Figure 11. Then, the LEM and NSM are used to verify the results under static conditions of GHSM. Among the LEM, the Morgenstern-Price method is adopted to evaluate the stability of slopes, which is more rigorous than other LEM because it considers both the balance of forces and moments. In the NSM, the commercial software FLAC³ᴰ is used to obtain the safety factor and potential sliding surface. In the FLAC³ᴰ, the safety factor and corresponding sliding surface by the SSR technique are related only to the cohesion and inter-
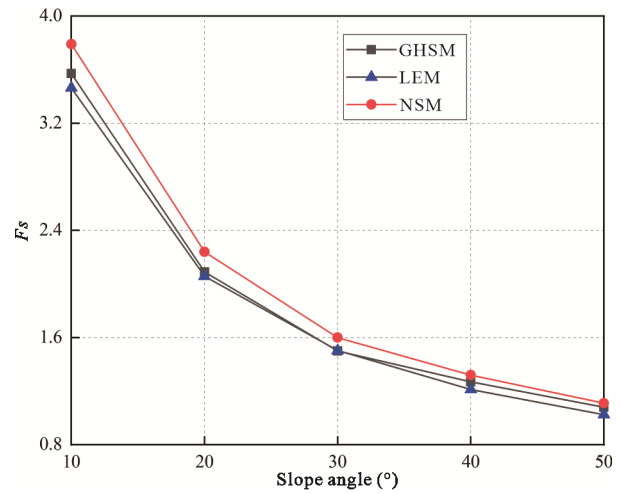

Figure 10. Static safety factor F_s with different slope angle β.

Table 2 Calculated results of generalized horizontal slice, polar slice, and Chen's methods (Chen et al., 2017)

Failure mode	GHSM ($N = 8$)		Polar slice method ($N = 10$)		Chen's method	
	F_{s1}	k_{h1}	F_{s2}	k_{h2}	F_{s4}	k_{h4}
Mode A	1.212 0	0.160 7	1.203 0	0.145 0	1.108 0	0.084 4
Mode B	1.629 0	0.653 4	1.566 8	0.373 8	1.402 4	0.260 5

Mode A. passing through the toe of slope; mode B. passing below the toe of slope.

Table 3 The soil parameters of the multi-layer slope (from Wang, 2018)

Layer	ρ (g/cm³)	c (kPa)	φ (°)
1	1.87	13.12	19.10
2	1.89	14.29	19.37
3	1.92	14.41	19.69
4	1.98	15.34	19.85
5	2.01	15.34	19.77
6	2.15	16.44	20.49

nal frictional angle, while other parameters, such as the bulk modulus and shear modulus, just affect the deformation rather than the safety factor. The aforementioned parameters in Table 3 are considered, and other parameters that do not affect the strength reduction technique are determined with values as follows: bulk modulus $K = 1\,000$ MPa and shear modulus $G = 300$ MPa. The results of the safety factor of LEM and NSM are shown by the blue and red line in Figure 10, and the potential sliding surfaces of that are presented by the blue and magenta line in Figure 11, respectively.

Figure 10 indicates that the results of the safety factor under the static conditions of GHSM, LEM and NSM are very close, and the margin of error is within 5%. This proves the applicability of GHSM in the multi-layer slopes. Figure 11 shows that the ultimate sliding surfaces of the GHSM, LEM and NSM have the same failure mode in each case. In addition, Figures 11a and 11b show that both methods obtain the ultimate failure mode of passing below the toe of the slope (mode B)
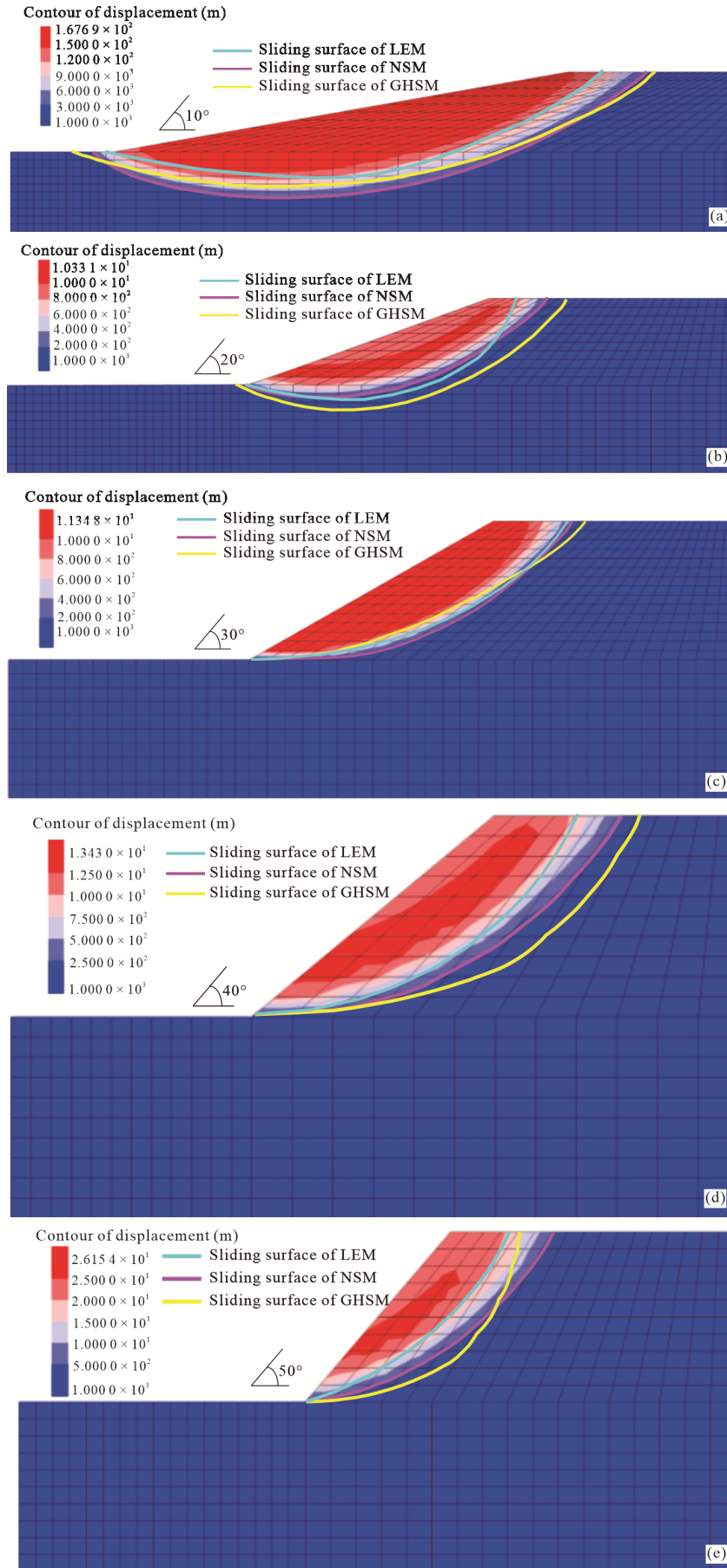
Figure 11. Sliding surface with different slope angle β; (a) $\beta = 10°$; (b) $\beta = 20°$; (c) $\beta = 30°$; (d) $\beta = 40°$; (e) $\beta = 50°$.

when the slope angle is not more than 20°. On the contrary, Figures 11c−11e show the ultimate failure modes are the sliding surface passing through the toe of slope (mode A) when slope angle is not less than 30°.

To further analyze the effect of slope angle on the failure mode of the multi-layer slope, the slope angle is divided by spacing for 1° from 21° to 29°, which can determine the critical slope angle to distinguish mode A and mode B in this example. The stability of the multi-layer slope with the slope angle from 21° to 29° is solved by GHSM, LEM and NSM. The sliding surfaces of the slope angles of 28° and 29° are shown in Figure 12. The ultimate failure mode is mode B when the slope angle is 28° and it is mode A when the slope angle is 29°, so the critical slope angle is determined to be 28° in this example. It illustrates that the determination of the ultimate sliding surface requires comparison of multiple failure modes, not only passing through the toe of slope (mode A).

3 DISCUSSION

On the basis of the GHSM, this paper derives a formula to assess the slope stability analysis considering the energy dissipation between the adjacent horizontal slices. The values of the soil parameters between adjacent horizontal slices are assumed to be the smaller values of the upper and lower layers. If there are no testing values, this assumption is feasible (Chen et al., 2017; Michalowski, 1995), but it is better to use tests to measure the values.

Additionally, this study carries out upper-bound limit analysis on homogeneous and multi-layer slopes and obtains that the sliding surfaces of the slope pass below the toe of the slope when the slope angle is small. This shows that when the slope angle is small, it is necessary to focus on the failure mode (mode B). This agrees with previous research conclusions (Kumar and Samui, 2006).

For the layered slope, based on the limiting equilibrium method, some scholars (Deng et al., 2019; Qiu and Wang, 2018; Deng and Li, 2012) have also used different methods to divide the sliding soil mass, including horizontal slice method, oblique slice method and the combination of several methods et al. Especially, Deng et al. (2012) and Qiu and Wang (2018) have adopted a combination of horizontal slice method and oblique slice method to analyze the slope stability when the sliding surface passing below the slope toe. These methods are worth applying to subsequent study of limit analysis.

This article considers the condition of the sliding surface passing below the toe of the slope, but this assumes that the soil layer under the ground is homogeneous and does not consider the conditions of multiple soil layers underground. Additionally, although this paper compares the sliding surface passing through the toe of the slope (mode A) with that below (mode B), the slope may also exhibit local instability failure; that is, the sliding surface passes the face of the slope which is worth studying. Moreover, the effects of other factors (e. g., groundwater and loading conditions) on slope stability are not the focus of this paper. Therefore, these factors will be comprehensively studied in more detail in the future.

4 CONCLUSIONS

Rapid urbanization generates a large amount of clay residue that is deposited by layers in receiving fields, forming multi-layer slopes. To further analyze the stability and failure mode of the multi-layer slope, a GHSM based on the upper-bound limit analysis is presented in this paper, which divides the sliding soil mass into several horizontal slices and its energy equation is derived by considering the energy dissipation between adjacent horizontal slices. In the GHSM, the stability coefficient and failure mode are determined by comparing the sliding surface passing through the toe of the slope (mode A) with that below it (mode B). Based on the harmony search algorithm, the stability coefficient and failure mode are solved by independent programming of MATLAB. Main conclusions are summarized as follows.
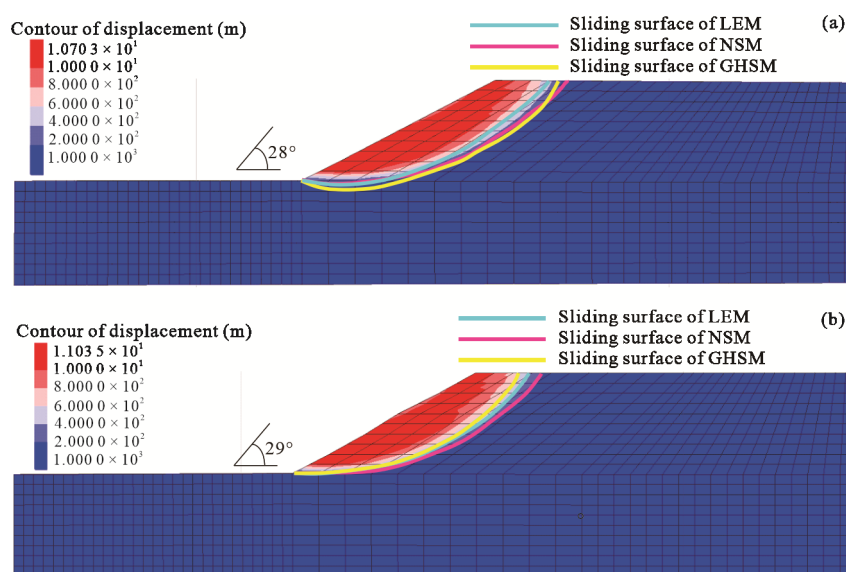

Figure 12. Sliding surface with different slope angle β; (a) $\beta = 28°$, (b) $\beta = 29°$.

(1) The influence of the number of slices N on the results of stability coefficients in the GHSM is studied. When N is not less than 8, the stability coefficients of modes A and B can reach stable values.

(2) Compared to traditional Chen's method, the GHSM can acquire more accurate results, which takes into account the energy dissipation in the inner sliding soil mass.

(3) The GHSM is applied to analyze the stability of a multi-layer slope and the results are very close to the LEM and NSM. The ultimate failure modes are shown to be mode B when the slope angle is not more than 28°. It illustrates that the determination of the ultimate sliding surface requires comparison of multiple failure modes, not only mode A.

ACKNOWLEDGMENTS

Conflict of Interest

The authors declare that they have no conflict of interest.

REFERENCES CITED

Ausilio, E., Conte, E., Dente, G., 2001. Stability Analysis of Slopes Reinforced with Piles. *Computers and Geotechnics*, 28(8): 591–611. https://doi.org/10.1016/s0266-352x(01)00013-1

Bishop, A. W., 1955. The Use of the Slip Circle in the Stability Analysis of Slopes. *Géotechnique*, 5(1): 7–17. https://doi.org/10.1680/geot.1955.5.1.7

Chang, C. J., Chen, W.-F., Yao, J. T. P., 1984. Seismic Displacements in Slopes by Limit Analysis. *Journal of Geotechnical Engineering*, 110(7): 860–874. https://doi.org/10.1061/(asce)0733-9410(1984)110:7(860)

Chen, C. S., Xia, Y. Y., Bowa, V. M., 2017. Slope Stability Analysis by Polar Slice Method in Rotational Failure Mechanism. *Computers and Geotechnics*, 81: 188–194. https://doi.org/10.1016/j.compgeo.2016.08.016

Chen, G. H., Zou, J. F., Pan, Q. J., et al., 2020. Earthquake-Induced Slope Displacements in Heterogeneous Soils with Tensile Strength Cut-off. *Computers and Geotechnics*, 124: 103637. https://doi.org/10.1016/j.compgeo.2020.103637

Chen, W. F., 1975. Limit Analysis and Soil Plasticity. Elsevier Science, Amsterdam

Chen, W. F., Giger, M. W., 1971. Limit Analysis of Stability of Slopes. *Journal of the Soil Mechanics and Foundations Division*, 97(1): 19–26. https://doi.org/10.1061/jsfeaq.0001515

Chen, W. F., Liu, X. L., 1990. Limit Analysis in Soil Mechanics. Elsevier, Amsterdam

Chen, W. F., Sawada, T., 1983. Earthquake-Induced Slope Failure in Nonhomogeneous, Anisotropic Soils. *Soils and Foundations*, 23(2): 125–139. https://doi.org/10.3208/sandf1972.23.2_125

Chen, W. Q., Song, Y. J., Wu, Z. B., et al., 2021. Stability of Double-Step Muck Slope under Different Overload Conditions. *European Journal of Environmental and Civil Engineering*, 25(2): 245–263. https://doi.org/10.1080/19648189.2018.1526120

Cheng, Y. M., Li, D. Z., Li, L., et al., 2011. Limit Equilibrium Method Based on an Approximate Lower Bound Method with a Variable Factor of Safety that can Consider Residual Strength. *Computers and Geotechnics*, 38(5): 623–637. https://doi.org/10.1016/j.compgeo.2011.02.010

Cui, P., Peng, J. B., Shi, P. J., et al., 2021. Scientific Challenges of Research on Natural Hazards and Disaster Risk. *Geography and Sustainability*, 2(3): 216–223. https://doi.org/10.1016/j.geosus.2021.09.001

Deng, D. P., Li, L. A., Zhao, L. H., 2019. Stability Analysis of a Layered Slope with Failure Mechanism of a Composite Slip Surface. *International Journal of Geomechanics*, 19(6): 04019050. https://doi.org/10.1061/(asce)gm.1943-5622.0001417

Deng, D. P., Li, L., 2012. Analysis of Slope Stability and Research of Calculation Method under Horizontal Slice Method. *Rock and Soil Mechanics*, 33(10): 3179–3188. https://doi.org/10.16285/j.rsm.2012.10.020 (in Chinese with English Abstract)

Drucker, D. C., Prager, W., Greenberg, H. J., 1952. Extended Limit Design Theorems for Continuous Media. *Quarterly of Applied Mathematics*, 9(4): 381–389. https://doi.org/10.1090/qam/45573

Fang, K., Tang, H. M., Zhu, J. C., et al., 2023. Study on Geomechanical and Physical Models of Necking-Type Slopes. *Journal of Earth Science*, 34(3): 924–934. https://doi.org/10.1007/s12583-021-1573-1

Farshidfar, N., Keshavarz, A., Mirhosseini, S. M., 2020. Pseudo-Static Seismic Analysis of Reinforced Soil Slopes Using the Horizontal Slice Method. *Arabian Journal of Geosciences*, 13(7): 1–14. https://doi.org/10.1007/s12517-020-5269-0

Fellenius, W., 1927. Earth Stability Calculations Assuming Friction and Cohesion on Circular Slip Surfaces. W. Ernst, Berlin

Gao, Y., Yin, Y. P., Li, B., et al., 2017. Investigation and Dynamic Analysis of the Long Runout Catastrophic Landslide at the Shenzhen Landfill on December 20, 2015, in Guangdong, China. *Environmental Earth Sciences*, 76(1): 1–16. https://doi.org/10.1007/s12665-016-6332-8

Geem, Z. W., Kim, J. H., Loganathan, G. V., 2001. A New Heuristic Optimization Algorithm: Harmony Search. *Simulation*, 76(2): 60–68. https://doi.org/10.1177/003754970107600201

Guo, S. F., Griffiths, D. V., 2020. Failure Mechanisms in Two-Layer Undrained Slopes. *Canadian Geotechnical Journal*, 57(10): 1617–1621. https://doi.org/10.1139/cgj-2019-0642

Kamran, M., Hu, X. W., Hussain, M. A., et al., 2023. Dynamic Response and Deformation Behavior of Kadui-2 Landslide Influenced by Reservoir Impoundment and Rainfall, Baoxing, China. *Journal of Earth Science*, 34(3): 911–923. https://doi.org/10.1007/s12583-022-1649-6

Kumar, J., Samui, P., 2006. Stability Determination for Layered Soil Slopes Using the Upper Bound Limit Analysis. *Geotechnical & Geological Engineering*, 24(6): 1803–1819. https://doi.org/10.1007/s10706-006-7172-1

Li, C. C., Jiang, P. M., 2020. Failure Mechanism of Two-Layered Slopes Subjected to the Surcharge Load. *International Journal of Geomechanics*, 20(2): 06019024. https://doi.org/10.1061/(asce)gm.1943-5622.0001579

Li, C. D., Chen, W. Q., Song, Y. J., et al., 2020. Optimal Location of Piles in Stabilizing Slopes Based on a Simplified Double-Row Piles Model. *KSCE Journal of Civil Engineering*, 24(2): 377–389. https://doi.org/10.1007/s12205-020-0712-z

Li, C. D., Criss, R. E., Fu, Z. Y., et al., 2021. Evolution Characteristics and Displacement Forecasting Model of Landslides with Stair-Step Sliding

Surface along the Xiangxi River, Three Gorges Reservoir Region, China. *Engineering Geology*, 283: 105961. https://doi. org/10.1016/j. enggeo.2020.105961

Li, C. D., Fu, Z. Y., Wang, Y., et al., 2019. Susceptibility of Reservoir-Induced Landslides and Strategies for Increasing the Slope Stability in the Three Gorges Reservoir Area: Zigui Basin as an Example. *Engineering Geology*, 261: 105279. https://doi. org/10.1016/j. enggeo. 2019.105279

Li, X. P., He, S. M., Wu, Y., 2010. Seismic Displacement of Slopes Reinforced with Piles. *Journal of Geotechnical and Geoenvironmental Engineering*, 136(6): 880–884. https://doi. org/10.1061/(asce)gt. 1943-5606.0000296

Lim, K., Li, A. J., Schmid, A., et al., 2017. Slope-Stability Assessments Using Finite-Element Limit-Analysis Methods. *International Journal of Geomechanics*, 17(2): 06016017. https://doi. org/10.1061/(asce) gm.1943-5622.0000715

Liu, F., Rui, Y. Q., Zhang, C., 2017. Three Dimensional Limit Analysis of Slope Stability with Nonlinear Criterion: Comparison the Effect of Volumetric Strain. *Indian Geotechnical Journal*, 47(1): 57–66. https:// doi.org/10.1007/s40098-016-0193-7

Lo, S. C. R., Xu, D. W., 1992. A Strain-Based Design Method for the Collapse Limit State of Reinforced Soil Walls or Slopes. *Canadian Geotechnical Journal*, 29(5): 832–842. https://doi.org/10.1139/t92-090

Ma, C. H., Yang, J., Cheng, L., et al., 2022. Research on Slope Reliability Analysis Using Multi-Kernel Relevance Vector Machine and Advanced First-Order Second-Moment Method. *Engineering with Computers*, 38(4): 3057–3068. https://doi. org/10.1007/s00366-021-01331-9

Michalowski, R. L., 1995. Slope Stability Analysis: A Kinematical Approach. *Géotechnique*, 45(2): 283–293. https://doi. org/10.1680/ geot.1995.45.2.283

Michalowski, R. L., 1998. Soil Reinforcement for Seismic Design of Geotechnical Structures. *Computers and Geotechnics*, 23(1/2): 1–17. https://doi.org/10.1016/s0266-352x(98)00016-0

Michalowski, R. L., You, L. Z., 2000. Displacements of Reinforced Slopes Subjected to Seismic Loads. *Journal of Geotechnical and Geoenvironmental Engineering*, 126(8): 685–694. https://doi. org/10.1061/(asce) 1090-0241(2000)126:8(685)

Qin, C. B., Chian, S. C., 2017. Kinematic Stability of a Two-Stage Slope in Layered Soils. *International Journal of Geomechanics*, 17(9): 06017006. https://doi.org/10.1061/(asce)gm.1943-5622.0000928

Qiu, C., Wang, P. A., 2018. Analytical Calculation for Slope Stability Based on the Combination of Horizontal Slice Method and Oblique Slice Method. *IOP Conference Series*: *Materials Science and Engineering*, 307: 012059. https://doi.org/10.1088/1757-899x/307/1/012059

Shahgholi, M., Fakher, A., Jones, C. J. F. P., 2001. Horizontal Slice Method of Analysis. *Géotechnique*, 51(10): 881–885. https://doi.org/10.1680/ geot.2001.51.10.881

Shield, R. T., Drucker, D. C., 1953. The Application of Limit Analysis to Punch-Indentation Problems. *Journal of Applied Mechanics*, 20(4): 453–460. https://doi.org/10.1115/1.4010747

Su, A. J., Feng, M. Q., Dong, S., et al., 2022. Improved Statically Solvable Slice Method for Slope Stability Analysis. *Journal of Earth Science*, 33(5): 1190–1203. https://doi.org/10.1007/s12583-022-1631-3

Tang, H. M., Li, C. D., Hu, W., et al., 2022. What is the Physical Mechanism of Landslide Initiation? *Earth Science*, 47(10): 3902–3903. https://doi. org/10.3799/dqkx.2022.857 (in Chinese)

Wang, C. Q., 2018. Study on Failure Mechanism and Control Structures Optimizing Design of Complex Multi-Layer Sediment Receiving Field Slope under Rainfall Conditions: [Dissertation]. China University of Geosciences, Wuhan (in Chinese with English Abstract)

Wang, H. Y., Huang, M. S., 2020. Upper Bound Stability Analysis of Slurry-Supported Trenches in Layered Soils. *Computers and Geotechnics*, 122: 103554. https://doi.org/10.1016/j.compgeo.2020.103554

Wang, L. Q., Yin, Y. P., Huang, B. L., et al., 2020. Damage Evolution and Stability Analysis of the Jianchuandong Dangerous Rock Mass in the Three Gorges Reservoir Area. *Engineering Geology*, 265: 105439. https://doi.org/10.1016/j.enggeo.2019.105439

Wang, L., Yang, R. X., Xu, Y., et al., 2013. An Improved Adaptive Binary Harmony Search Algorithm. *Information Sciences*, 232: 58–87. https:// doi.org/10.1016/j.ins.2012.12.043

Wang, Z., Yang, X. M., Li, A., 2020. Upper Bound Limit Stability Analysis for Soil Slope with Nonuniform Multiparameter Distribution Based on Discrete Algorithm. *Advances in Civil Engineering*, (4): 1–9. https:// doi.org/10.1155/2020/7452656

Xia, Y. Y., Chen, C. S., 2017. Limit Analysis of Reinforced Slopes with Prestressed Anchor Cables Considering Energy Dissipation Due to Deformation of Inner Friction. *Chinese Journal of Geotechnical Engineering*, 39(2): 210–217. https://doi.org/10.11779/cjge201702003 (in Chinese with English Abstract)

Xia, Y. Y., Chen, C. S., 2018. Seismic Stability Limit Analysis of Reinforced Soil Slopes with Prestressed Cables Considering Inhomogeneity and Anisotropy of Multiple Parameters. *Chinese Journal of Rock Mechanics and Engineering*, 37(4): 829–837. https://doi.org/10.13722/ j.cnki.jrme.2017.1283 (in Chinese with English Abstract)

Yan, M. J., Xia, Y. Y., Liu, T. T., et al., 2019. Limit Analysis under Seismic Conditions of a Slope Reinforced with Prestressed Anchor Cables. *Computers and Geotechnics*, 108: 226–233. https://doi.org/10.1016/j. compgeo.2018.12.027

Zhang, H. W., Li, C. D., Xie, N., et al., 2023. Characterization of Macro- and Meso-Scale Shear Behavior of Soil-Brick Mixtures with Different Contents and Shapes of Brick by Discrete Element Method. *Journal of Earth Science*, 34(5): 1641–1644. https://doi.org/10.1007/s12583-023-1942-x

Zhong, Y., Li, Y. Y., Yin, K. L., et al., 2023. Failure Mechanism of Thick Colluvium Landslide Triggered by Heavy Rainfall Based on Model Test. *Earth Science*, 48(10): 3912–3924. https://doi.org/10.3799/dqkx. 2021.248 (in Chinese with English Abstract)

Zhou, A. Z., Liu, G., Huang, X. W., et al., 2020. Stability Analysis of a Two-Layered Slope with Cracks by Finite Element Limit Analysis. *Advances in Civil Engineering*, (5): 1–15. https://doi.org/10.1155/2020/ 8812277

Zhou, H. F., Ye, F., Fu, W. X., et al., 2024. Dynamic Effect of Landslides Triggered by Earthquake: A Case Study in Moxi Town of Luding County, China. *Journal of Earth Science*, 35(1): 221–234. https://doi. org/10.1007/s12583-022-1806-y